Steel and Composite Structures, *Vol. 30, No. 1* (*2019*) *69-79*
DOI: https://doi.org/10.12989/scs.2019.30.1.069

Strengthening of deficient steel SHS columns under axial compressive loads using CFRP

Mehdi Shahraki [1a], Mohammad Reza Sohrabi [1b], Gholamreza Azizyan [1c] and Kambiz Narmashiri [*2]

[1] *Department of Civil Engineering*, *University of Sistan and Baluchestan*, *Zahedan*, *Iran*
[2] *Department of Civil Engineering*, *Zahedan Branch*, *Islamic Azad University*, *Zahedan*, *Iran*

(*Received January 17, 2018, Revised December 6, 2018, Accepted January 15, 2019*)

Abstract. Numerous problems have always vexed engineers with buckling, corrosion, bending, and over-loading in damaged steel structures. The present study aims to study the possible effects of Carbon Fiber Reinforced Polymer (CFRP) for strengthening deficient Steel Square Hollow Section (SHS) columns. To this end, the effects of axial loading, stiffness values, axial displacement, the shape of deficient on the length of steel SHS columns were evaluated based on a detailed parametric study. Ten specimens were tested to failure under axial compression in laboratory and simulated by using Finite Element (FE) analysis based on numerical approach. The results indicated that the application of CFRP sheets resulted in reducing stress in the damage location and preventing or retarding local deformation around the deficiency location appropriately. In addition, the retrofitting method could increase loading the carrying capacity of specimens.

Keywords: Square Hollow Section (SHS); deficiency; CFRP; steel column; strengthening

1. Introduction

Steel structures are one of the most commonly used structures Bambach and Elchalakani (2007). Erroneous, weak structure design/execution, poor steel bending/cutting details, poor stiffener reinforcing/placing, long-term static/dynamic loading fatigue, and so on create such problems as corrosion, cracks, and gaps in steel beam/column cross sections and cause the designed structure to be weak and apt to collapse. In the past, structures used to follow old standards and failed by such natural disasters as winds and earthquakes. Therefore, the need for improving and restoring is inevitable for the desired structures to tolerate the increased ultimate load and fatigue. Recently, using the synthetic Fiber Reinforced Polymer (FRP) composites in steel structures to retrofit and rehabilitate members has attracted much attention and since they do not need special equipment for welding operations, reduce fatigue in steel structures, have high speed performance, eliminate welding-caused problems, and remove stress concentration, they have been highlighted during recent years (Shahraki *et al*. 2018).

FRP composites are preferred to steel due to their high strength-to-weight ratio and optimal corrosion resistance. It is worth noting that steel plates can be adhesively bonded; although, bonding is less attractive for steel plates due to their heavy weight and inflexibility (Shahraki *et al*. 2018).

However external bonding of steel plates was efficient, it presented some problems such as increase of self-weight (dead load), required heavy lifting equipment to install the plates in position, and moreover added plates are susceptible to corrosion which causes an increase in future maintenance expenditures (Ghaemdoust *et al*. 2016). Such factors as humidity, salt concentration, and temperature can create a corrosive environment for welding and local heating/cooling during welding can produce a non-uniform temperature distribution causing high residual tensile stresses around the weld and the heat affected zones and can be the main source of tension in the metal corrosion. If sections put pressure on residual stresses from welding, crack propagation will be actuated (Kusnick *et al*. 2013).

Bambach *et al*. (2009) demonstrated that the axial capacity and the design of thin walled steel SHS were strengthen by using CFRP in describing 20 experiments on short, axially compressed square hollow sections (SHS) cold-formed from G450 steel and strengthened with externally bonded CFRP. Base on the results, the use of CFRP could double the axial capacity up to 2 times for the capacity of the steel section alone and enhance the strength to-weight ratio of up to 1:5 times. Therefore, CFRP can provide harness to the outreach of elastic buckling defections and accordingly reprieve local buckling. The related restraint provides an increase in the buckling stress up to four, compared to that of the steel section alone.

Teng *et al*. (2012) studied the steel structure strengthening with FRP composites and concluded that CFRP fibers could highly increase the resistance, yield, ultimate strength, and stiffness These fibers are regarded important for enhancing shear/tensile strength, and toughness, and since the rapture continuity level is important for steel beams bending strength and buckling of

*Corresponding author, Ph.D.,
E-mail: narmashiri@iauzah.ac.ir
[a] Ph.D., E-mail: m.shahraki@iauzah.ac.ir
[b] Ph.D., E-mail: sohrabi@hamoon.usb.ac.ir
[c] Ph.D., E-mail: azizian@hamoon.usb.ac.ir

ISSN: 1229-9367 (Print), 1598-6233 (Online)

thin walled steel buildings, adhesion and compressive loads should be examined to overcome the material parameters.

Regarding the connections between RC beam and square tubed- RC column under axial compression with Zhou *et al*. (2017). They concluded that the stiffening fibers plays a significant role in improving the load-carrying capacity and ductility of the proposed connection type. Further, they found that the RC horizontal haunch can improve the ductility and ultimate axial loading of both exterior and corner connections.

Yang *et al*. (2017) evaluated the axial compression performance of reinforced steel box columns with experimental and numerical methods. Based on the results, the reinforcement scheme increased the axial stiffness, maximum axial load of the specimens and the improved reinforcement scheme can improve the load conditions of steel angles. Devi and Amanat (2015) investigated the behavior of (HSS) columns strengthened with CFRP. Further, they found that the CFRP materials are capable of increasing the axial load capacity of the steel HSS columns. In another study, Narmashiri *et al*. (2010) examined I-shaped retrofitted shear resistance of steel beams by implementing CFRP strips. The results indicated the shear reinforcement of steel beam as a successful method to increase the bearing capacity and reduce deformations. It is worth noting that steel plates can also be adhesively bonded; however, bonding is less attractive for steel plates due to their heavy weight and inflexibility. In such specific applications as oil storage tanks and chemical plants, where the fire risk is to be minimized, welding must be avoided while strengthening a structure. As a result, bonding of FRP laminates becomes a very promising alternative. High-strength steel suffers from significant local strength reduction in the heat-affected weld zone. Bonded FRP laminates offer an ideal strength compensation method (Dieng *et al*. 2017).

Park and Yoo (2015) discussed the experimental results of flexural and compression steel members strengthened by CFRP sheets. Among the four short columns, the two sides could typically buckle outward while the two other sides could buckle inward. Further, overall buckling was attended for long columns. Based on the results, a maximum increase of 57% was accomplished in axial-load carrying capacity when 3 sheets of CFRP were used to retrofit HSS columns of $b/t = 60$ transversely.

In another study, Park and Yoo (2013) emphasized on axially loaded stub columns of slender steel hollow square section (SHS) strengthened with CFRP sheets. To this aim, a total number of 9 specimens were analyzed and the role of With-thickness ratio (b/t), the number of CFRP plate, and sheet orientation on the ultimate load carrying capacity was evaluated. The results indicated that the use of CFRP layers to slender sections plays a significant role on delaying local buckling and increasing inelastic buckling stress.

Some researchers investigated the CFRP strengthening of notched damaged steel beam and columns. Den *et al*. (2016) focused on strengthening the notched steel beams by CFRP. Generally, premature debonding failure leading to stress concentration at the notch zone can diminish the efficiency of this strengthening method. Based on the experimental results, strengthening CFRP plate can double the strength of the damaged steel beam and accordingly the intermediate debonding initiated from the notch location can create brittle fracture leading to the reduction of the retrofitted beam ductility. Further, Ghaemdoust *et al*. (2016) in another study, highlighted the structural behaviors of deficient steel SHS short columns which were strengthened by CFRP. To this end, eight deficient specimens were repaired by using CFRP sheets. Based on the results, the application of CFRP sheets for strengthening deficient steel short SHS columns could significantly recover the strength-lost due to the deficiency. In addition, an increase occurred in the load bearing capacity and delaying local buckling. Yousefi *et al*. (2017) stressed the effect of CFRP strips on strengthening notched steel beams and concluded that CFRP plates can prevent crack propagation and brittle fractures in the deficiency region. In addition, Karimian *et al*. (2017) studied the effects of deficiency on reducing axial resistance and the possibility of overcoming weakness on CHS short columns strengthened using CFRP sheets. They considered CFRP layers as leading to reduced stress in the damage region, a higher load-carrying capacity, and the prevention of local buckling around the deficient region. Shahraki *et al*. (2018) published the results of an experimental and numerical investigation of strengthened deficient steel SHS columns using two methods: welding steel plate and wrapping by CFRP sheets under axial compression loads. The results confirmed that the CFRP layers have better performance than the steel plate for the strengthening of the deficient region on the specimens.

Previous works have just focused on application of CFRP in strengthening notched damage on short steel columns. In addition, no research appears to have surveyed the use of CFRP sheets on retrofitting deficient intermediate steel SHS column. The present study aimed to evaluate the role of CFRP in strengthening steel columns. Thus, the effect of CFRP layers for strengthening deficient steel SHS columns under axial compression loads was highlighted in the present study.

2. Materials and methods

2.1 Material properties

2.1.1 Steel columns

The section sizes employed for the SHS steel columns test were SHS 40×40×2 (mm) and SHS 80×80×2 (mm). The lengths of all steel columns were 2500 (mm). The boundary conditions of the specimens were designed to provide the fixed support by using one steel plate and four equal-leg angles welded at the end of columns. Prior to commencing the study, for investigating effect of the deficiency on the ultimate load-carrying capacity of the columns, five 80×80×2 (mm) columns with a slenderness ratio ($\lambda = \frac{k \times l}{r}$) equal to 33.5 and five 40×40×2 (mm) specimens with $\lambda = 80$ were used. (for intermediate columns: $\lambda < \lambda_C$; $\lambda_C = \frac{k \times l}{r}\sqrt{\frac{F_y}{\pi^2 E}} = 130$). The effective length factor (k) was assumed to be 0.5. After comparing

Table 1 Material properties of steel plate and columns

Steel hollow section columns specifications				Modulus of elasticity (MPa)	Stress (MPa)		Elongation (%)
Specimen label	Thickness (mm)	Height (mm)	Deficient cross sectional area (mm^2)		Yield stress	Ultimate stress	
BOX40 & BOX80	2	2500	800 & 3200	219267	366	398	15.794

the effect of cross-section, and shape of damage, two kinds of defects were identified: (a) a rectangular deficient region with a specified dimension in the middle of the length column; and (b) a circular deficient region with the same area and position as the rectangular deficient region. In the end, two columns were improved without retrofitting and the other columns were strengthened using CFRP sheets. The layer cover of CFRP in the deficiency area can be twice as much as that of the vertical height of the defects. Material properties, SHS steel column information, and steel plate tensile test results (based on ASTMA370 and AASHTOT299) are shown in Table 1. Figs. 1 and 2 present the defect-related data and specimens' section dimensions and Figs. 3 and 4 show the tensile coupon test configuration and the tested stress-strain curves, respectively. Terms used for the specimens include BOX = Steel SHS Column; DMG = Deficient; MID = Middle; REC = Rectangular Deficient; CIR = Circular Deficient.

2.1.2 CFRP

The CFRP used in this study is unidirectional Sikawrap 230-C (Sikawrap-230C 2006). The properties of the carbon fiber supplied by the manufacturer are indexed in Table 2.

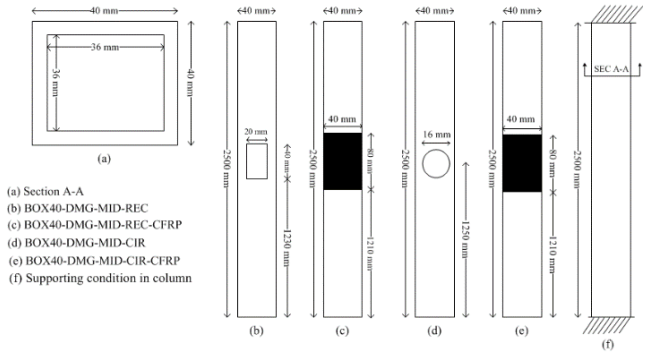

Fig. 1 Measured geometric dimensions of the BOX40

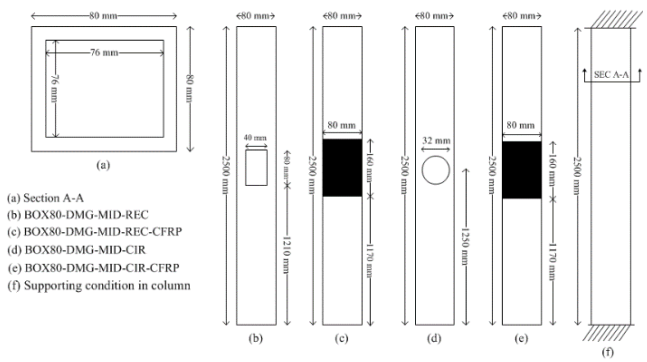

Fig. 2 Measured geometric dimensions of the BOX80

2.1.3 Adhesive

Adhesive supplies the power transmission path between the steel and composite materials. Adhesive causes the identical performance of composite and columns. CFRP sheets are attached to the steel columns by using Sikadur-330 epoxy (Sikadur-330 2012). Table 3 indicates the epoxy used by the supplier of CFRP as the proposed product.

2.2 Research methods

2.2.1 Experimental specimens preparation

A total of 10 column specimens were prepared (Fig. 5) and defects were created in them by the Computer Numerical Control (CNC) machine (Fig. 5(a)) and all the external roughness, loose steel particles, and grease were removed by sandblasting, acetone, and cotton (Figs. 5(d) and (e)). Then, CFRP sheets were cut into proper dimensions and wrapped around the defective areas on steel SHS columns by two longitudinal and two transverse layers

Fig. 3 Measured local geometric imperfection

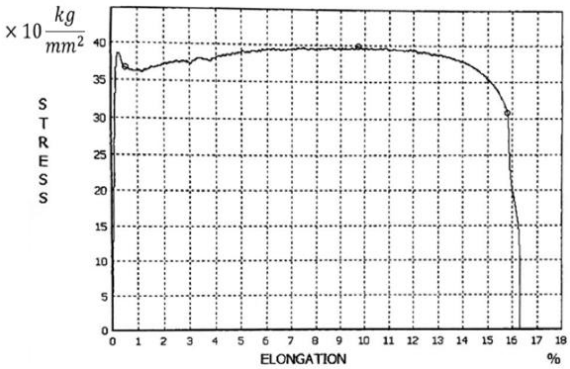

Fig. 4 Stress-strain curve for steel material

Table 2 Material properties of CFRP sheets (Sikawrap-230C 2006)

Tensile strength (MPa)	Tensile E-modulus (MPa)	Ultimate strain (%)	Thickness (mm)	Width (mm)
4300	238000	1.8	0.131	500

Table 3 Properties of the adhesive Sikadur-330 (2012)

Tensile strength (MPa)	Flexural E-nodulus (MPa)	Tensile E-modulus (MPa)	Elongation at break (%)
30	3800	4500	0.9

according to the manufacturer's instructions regarding overlapping conditions and adhesive geometrical mix design (Fig. 5(f)). Finally, the specimens were kept in the laboratory at the room temperature for at least one week before testing. Tests were performed in the Structural Engineering Department Lab, Islamic Azad University (Zahedan, Iran), and the specimens were loaded up to failure under a uniform uniaxial compressive load by a hydraulic universal testing machine with a vertical load capacity of 1000 kN. The load was applied trough using a hydraulic jack that includes a load cell of $450\,kN$ capacity. the load bearing capacity (P_{cr}) and maximum axial displacement ($\delta_{\max}$) were measured by the Linear Variable Differential Transformer (LVDT) connected to the column top. The load cell and LVDT were connected to

Fig. 5 Preparation of CFRP-strengthened specimens

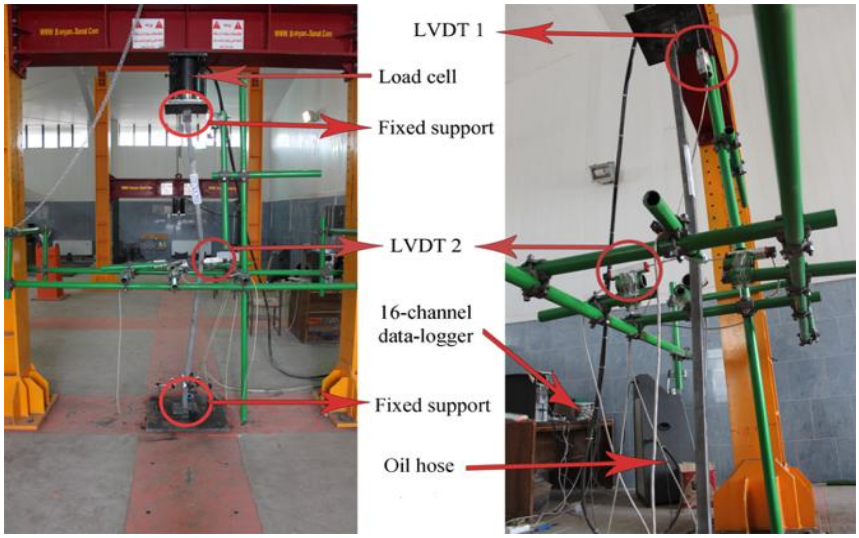

Fig. 6 Test setup for local/overall buckling

a 16-channel data-logger to save and record the data (Fig. 6). The load was gradually imposed by the jack. The test method was load-control type and the minimum loading rate was used. When the ultimate load was decreased suddenly by 20%, then the loading was stopped automatically due to safety. Afterward, the manual loading method can be used. Force gauge and LVDT are eclectically transducers that convert the force of jack and the displacement into voltage or electric current. Changes in voltage or electric current transmitted to the channels of data recording devices, then the amount of force and displacement will be displayed as a number by applying different calibration factor for each channel.

2.2.2 FE Simulation

In the present study, the ABAQUS ver. 6.14.1 was used to perform the FE analyses for the CFRP-strengthened steel SHS columns. To analyze the data and study the local buckling behavior of the SHS steel column, use was made of the CFRP, adhesive, and the 3D-8R node HEX element. Then, the statistical analysis simulation method was used to observe the plastic zone after post buckling. The material properties of CFRP sheets (Modulus of Elasticity = 238000 MPa, Tensile strength = 4300 MPa), adhesive (Modulus of Elasticity = 4500 MPa, Flexural E-Modulus = 3800 MPa), and yield stress (366 MPa), and ultimate strength (398 MPa) values of the SHS steel columns (Cross sectional area = 800 mm^2, Thickness = 2 mm, Height = 2500 mm, Modulus of Elasticity = 219267 MPa) were taken equal to those of the coupon test results and according to the properties of the manufacturer; Poisson's ratio was taken to be 0.3. To prevent the specimens' local buckling and end rotations and connect the adhesive and CFRP to the steel column (for proper surface interaction), use was made of an adequate fix-end-condition modelling of the end supports Park *et al*. (2013) and Tie Method, respectively. Materials with linear and nonlinear properties were defined; properties of the CFRP strips were defined as linear and orthotropic because they are unidirectional, and those of others were defined as nonlinear and isotropic Narmashiri and Jumaat (2011). The mesh size selected for this study was 10 mm (Fig. 7) and the ABAQUS software accuracy

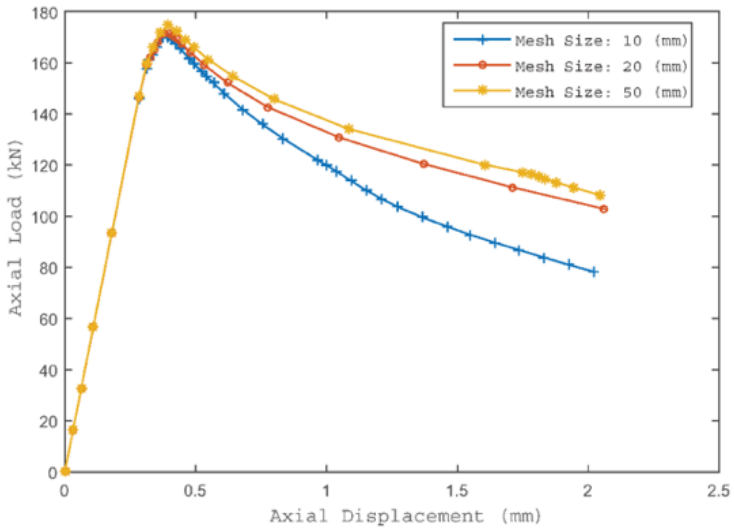

Fig. 7 Study on the mesh size

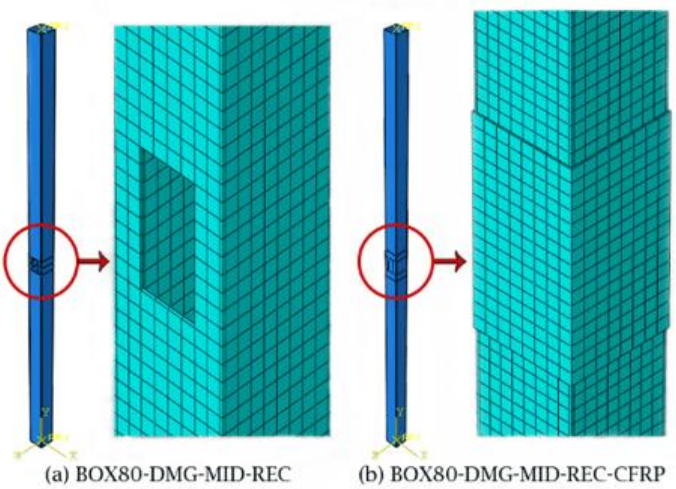

Fig. 8 The schematic of finite element modeling

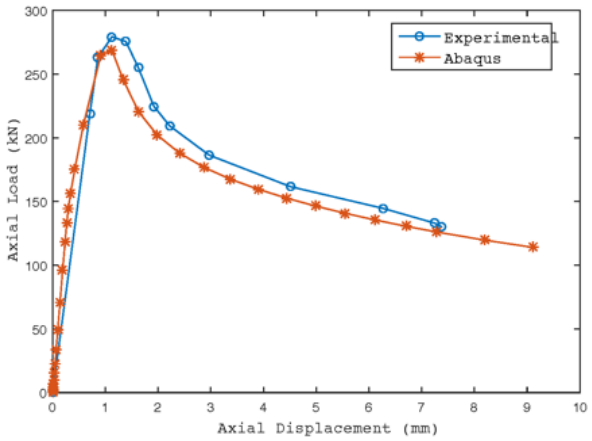

(a) BT100-0P

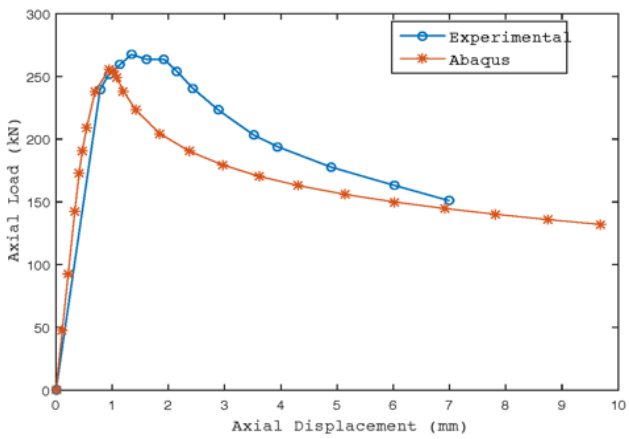

(b) BT80-1P

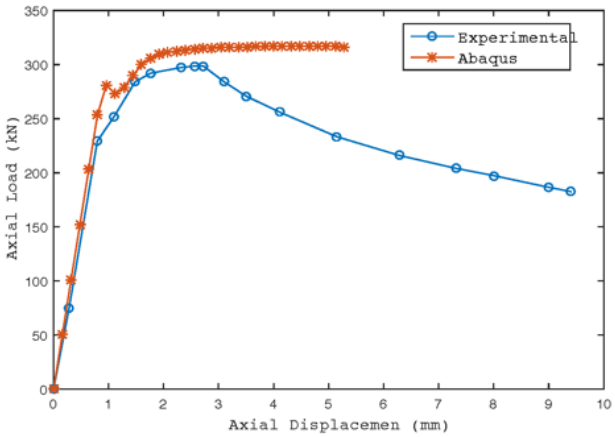

(c) BT80-3P

Fig. 9 Comparison of Load-Displacement curve results of FEM with experimental data of Park *et al*. (2013)

have been verified by the test results of the Park and Yoo (2015) study. The compatibility of 10 mm mesh modelling with laboratory specimen for both strengthened shows the correct selection of mesh, optimal boundary conditions, and appropriate software modelling. In this research, since the initial lab tests' imperfections are known to be similar to those of the tests on columns, a linear superposition of buckling Eigen modes were applied for parametric cases the buckling modes of which are unknown. Fig. 8 shows the schematic view of the FE modelling and Fig. 9 shows that the difference between the load and axial displacement for the specimens is minimal in both experimental and analytical software modes. As shown in Fig. 9, BT100-0P; BT: width-to-thickness ratio, (100, 80): $\frac{b}{t}$, 1P:1 transverse reinforcement ply.

3. Results and discussions

3.1 Behavior of columns in group #1

Group #1 included five columns, one of which were of the normal type of BOX40, and the rest had artificial defects, strengthened using CFRP. Fig. 10 and Table 4 provide the maximum load and stiffness of the columns.

Table 4 summarizes the results of maximum load obtained from tests and FEM analysis. Based on the results, a strong correlation was observed between the test and FEM results. the test maximum load values P_{Test} were quite to maximum load values P_{FEM} provided by FEM analysis as shown in Table 4. The mean and standard deviation of $P_{\frac{Test}{FEM}}$ ratio are 0.98698 and 0.033169, respectively. Stiffness is defined based on the Eq. (1). Fig. 11 illustrates the definition of stiffness. where $0.75P_{\max}$ is the axial load when the load reaches 75% of the maximum load in the pre-peak stage and $P_{\max}$ is regarded as the maximum load point. In addition, as shown in Fig. 11, P_k represents the load for the cross line point line (1) and (2). As indicated in Table 4, the values of test stiffness K_{Test} were almost close to the values of stiffness K_{FEM} provided by FEM analysis. In addition, the mean and standard deviation of the $K_{\frac{Test}{FEM}}$ ratio are 0.92689 and 0.055876, respectively. Further, creating rectangular deficient at the middle of the SHS columns is responsible for decreasing the maximum tolerable force by 48.27% and stiffness by 8.13% (Table 4). Additionally, 9.01% increase occurred in the maximum tolerable force by using CFRP, compared to the column with the rectangular defect. Load carrying capacity in columns with circular deficient at the middle caused

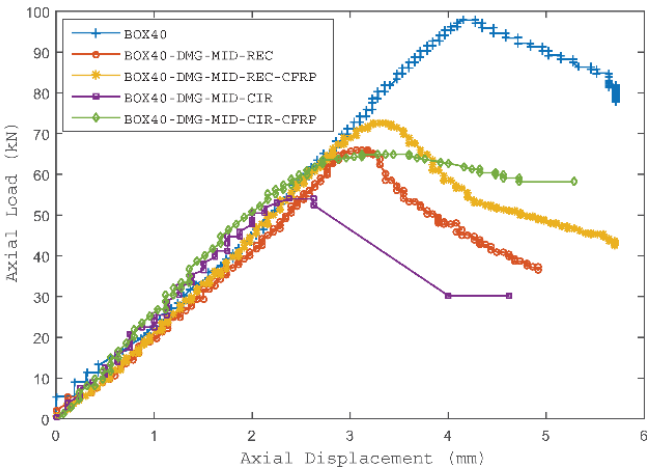

(a) Experimental Specimens of BOX40 strengthening with CFRP

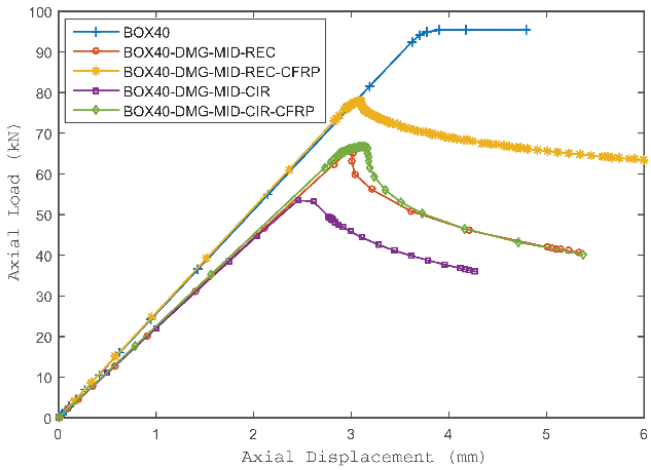

(b) Simulated Specimens of BOX40 strengthening with CFRP

Fig. 10 Comparison of test and simulated load displacement curves in BOX40 specimens

Table 4 Summery of test and FEM results in BOX40

Specimen label	Item	Results		Value of gain or loss		% gain or loss		Errors	
		Test	Fem	Test	Fem	Test	Fem	P (Test/Fem)	K (Test/Fem)
BOX40	Maximum load (kN)	97.86	95.48	Control	Control	Control	Control	1.02	-
BOX40	Stiffness $\left(\frac{\text{kN}}{\text{mm}}\right)$	22.87	22.88	Control	Control	Control	Control	-	0.99
BOX40-DMG-MID-REC	Maximum load (kN)	66.00	66.02	−31.86	−29.46	−48.27	−44.62	0.99	-
BOX40-DMG-MID-REC	Stiffness $\left(\frac{\text{kN}}{\text{mm}}\right)$	21.15	21.93	−1.72	−0.95	−8.13	−4.33	-	0.96
BOX40-DMG-MID-REC-CFRP	Maximum load (kN)	72.54	78.03	6.54	12.01	9.01	15.39	0.93	-
BOX40-DMG-MID-REC-CFRP	Stiffness $\left(\frac{\text{kN}}{\text{mm}}\right)$	21.98	26.01	0.83	4.08	3.92	18.60	-	0.85
BOX40-DMG-MID-CIR	Maximum load (kN)	54.00	53.50	−43.86	−41.98	−44.81	−43.96	1.00	-
BOX40-DMG-MID-CIR	Stiffness $\left(\frac{\text{kN}}{\text{mm}}\right)$	20.61	21.83	−2.26	−1.05	−9.88	−4.59	-	0.94
BOX40-DMG-MID-CIR-CFRP	Maximum load (kN)	64.98	66.74	10.98	13.25	16.89	1.92	0.97	-
BOX40-DMG-MID-CIR-CFRP	Stiffness $\left(\frac{\text{kN}}{\text{mm}}\right)$	18.88	21.39	−1.73	0.43	−8.39	1.97	-	0.88
Mean								0.98698	0.92689
St.dev								0.03316	0.05587

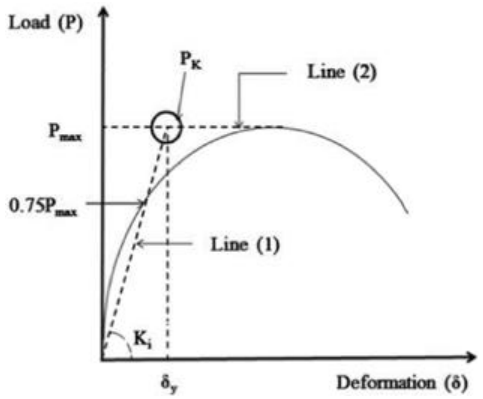

Fig. 11 Definition of stiffness Park *et al*. (2013)

a 44.81% decrease in maximum axial force, compared to the control sample. In addition, using CFRP is responsible for 16.89% increase, respectively. As shown in Table 4, the circular deficient in the middle of the column is regarded as the most critical mode, proving that the selected columns tend to buckle as they are slender.

$$K_i = \left(\frac{P_K}{\delta_y}\right) \tag{1}$$

Fig. 12 shows the support conditions in steel SHS columns. Fig. 13 illustrates the stress distribution around the rectangular deficient at the middle of the column due to the axial load applied by the jack in the laboratory. In general,

Fig. 12 Details of fixed supports in specimens

buckling is observable due to the low width/thickness : (b/t). Fig. 14 displays local and overall buckling around the region of deficient on steel column with circular defect in the middle of SHS. Further, Fig. 15 demonstrates the typical overall buckling in BOX40-DMG-MID-REC and CIR by using CFRP fibers.

3.3 Behavior of columns in group #2

Group #2 included five columns, one of which was of the normal type of BOX80, and the rest had artificial defects, strengthened using CFRP. Fig. 16 and Table 5 provide the maximum load and stiffness of the columns. Table 5 represents the results of load carrying capacity obtained from the tests and FEM analysis. As shown, a strong correlation was observed between test and FEM results. The values of the test maximum load P_{Test} are largely close to those provided by FEM analysis P_{FEM} (Table 5). The mean and standard deviation of $P_{\frac{Test}{FEM}}$ ratio are 1.0275 and 0.0156, respectively. As shown in Table 5, the test stiffness values K_{Test} were quite close to those provided by FEM analysis K_{FEM}. The mean and standard deviation of the $K_{\frac{Test}{FEM}}$ ratio are 1.0433 and 0.0491,

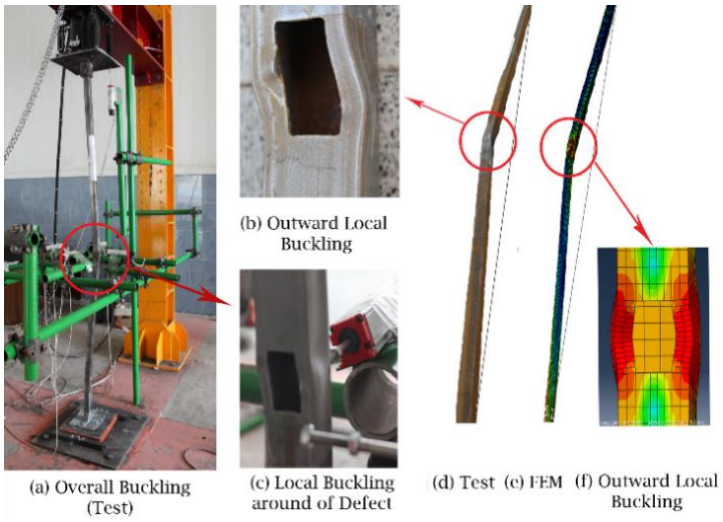

Fig. 13 Comparison of failure modes from the interactive buckling test and FE modelling in BOX40-DMG-MID-REC

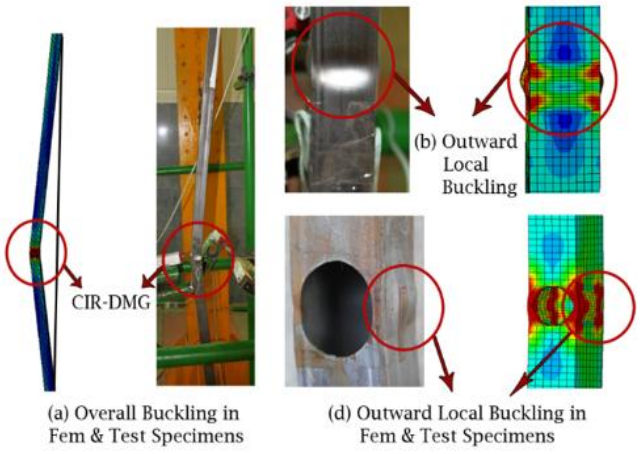

Fig. 14 Comparison of failure modes from the interactive buckling test and FEM modeling in BOX40-DMG-MID-CIR

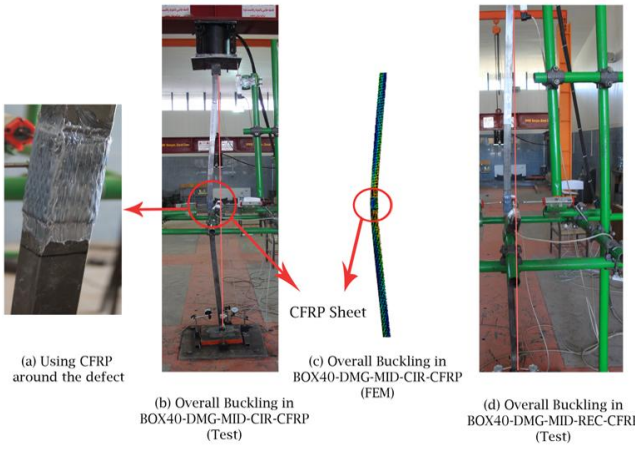

Fig. 15 Typical the overall buckling test and FEM modeling in BOX40-DMG-MID-REC & CIR using CFRP sheets

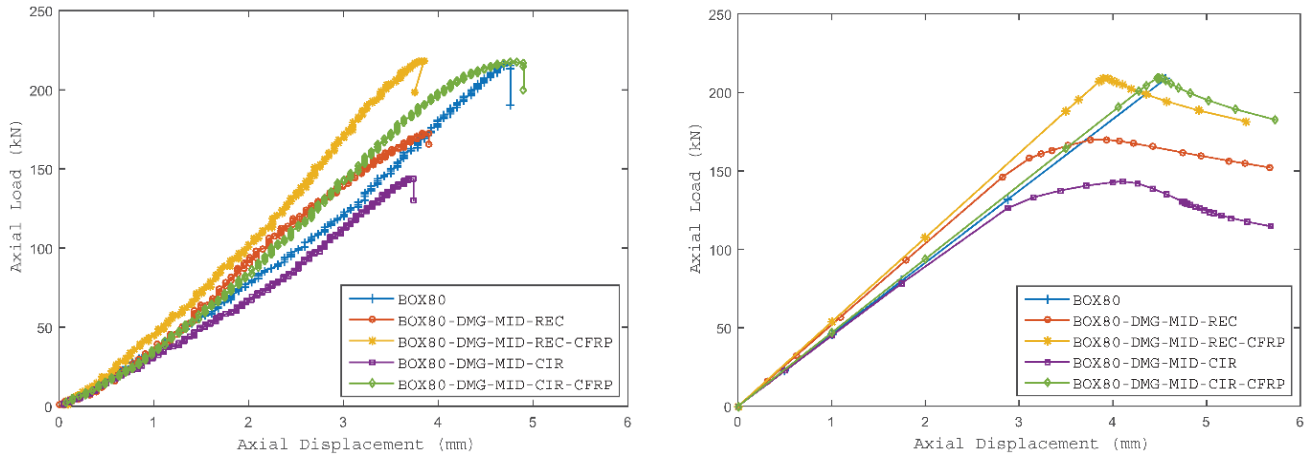

(a) Experimental specimens of BOX80 strengthening with CFRP (b) Simulated specimens of BOX80 strengthening with CFRP

Fig. 16 Comparison of test and simulated load displacement curves in BOX80 specimens

Table 5 Summery of test and FEM results in BOX80

Specimen label	Item	Results		Value of gain or loss		% gain or loss		Errors	
		Test	Fem	Test	Fem	Test	Fem	P (Test/Fem)	K (Test/Fem)
BOX80	Maximum load (kN)	215.82	208.71	Control	Control	Control	Control	1.03	-
BOX80	Stiffness $\left(\frac{\text{kN}}{\text{mm}}\right)$	46.01	45.76	Control	Control	Control	Control	-	1.00
BOX80-DMG-MID-REC	Maximum load (kN)	172.26	169.92	−43.56	−38.78	−25.28	−22.82	1.01	-
BOX80-DMG-MID-REC	Stiffness $\left(\frac{\text{kN}}{\text{mm}}\right)$	44.97	43.23	−1.04	−2.53	−2.31	−5.85	-	1.04
BOX80-DMG-MID-REC-CFRP	Maximum load (kN)	218.58	209.06	46.30	39.14	26.88	23.03	1.04	-
BOX80-DMG-MID-REC-CFRP	Stiffness $\left(\frac{\text{kN}}{\text{mm}}\right)$	56.76	53.06	11.79	9.83	26.21	22.73	-	1.07
BOX80-DMG-MID-CIR	Maximum load (kN)	143.80	143.13	−72.02	−65.58	−50.08	−45.81	1.00	-
BOX80-DMG-MID-CIR	Stiffness $\left(\frac{\text{kN}}{\text{mm}}\right)$	39.07	34.86	−6.94	−10.90	−17.76	−31.26	-	1.12
BOX80-DMG-MID-CIR-CFRP	Maximum load (kN)	217.62	209.32	73.82	66.19	51.33	46.24	1.04	-
BOX80-DMG-MID-CIR-CFRP	Stiffness $\left(\frac{\text{kN}}{\text{mm}}\right)$	45.71	46.61	6.64	11.75	16.99	33.70	-	0.98
Mean								1.0275	1.0433
St.dev								0.0156	0.0491

respectively. As observed in Table 5, a slight difference was found between the experimental and numerical (ABAQUS) results in terms of maximum load carrying capacity and column stiffness. In addition, rectangular deficient at the middle of the column is responsible for 25.28% tolerable force while the circular deficient in the middle of steel column causes 50.08% decline in tolerable force, compared to the control sample. A retrofitting thin-walled steel column with rectangular deficient at a middle of the column results in increasing the axial load carrying capacity by 26.88% Further, using CFRP is responsible for 51.33%, increase in load carrying capacity in columns with circular deficient in the middle, compared to the column without retrofitting, respectively. As expected, the increase in width/thickness: (b/t) ratio of BOX80 compared to BOX40 causes the tendency of greater local buckling at cross section. Further, no significant difference was observed in terms of tolerable force in BOX80 retrofitted with CFRP. Fig. 17 displays the overall-outward local buckling and deformation around the rectangular deficient and stress concentration in BOX80. As observed in Fig. 18, using CFRP sheets prevents deformation around deficient and deformation caused by local buckling. Finally, overall-local buckling details in BOX80 with circular deficient in the middle of column strengthened by CFRP fibers are illustrated in Fig. 19.

3.4 Failure modes

All the specimens were evaluated under axial compres-

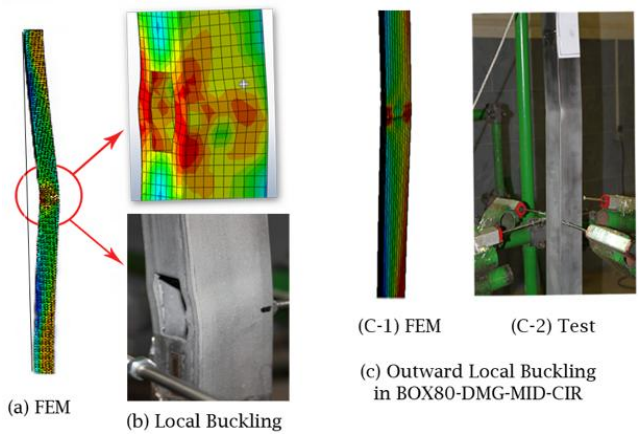

Fig. 17 Typical failure mode in BOX80-DMG-MID-REC & BOX80-DMG-MID-CIR

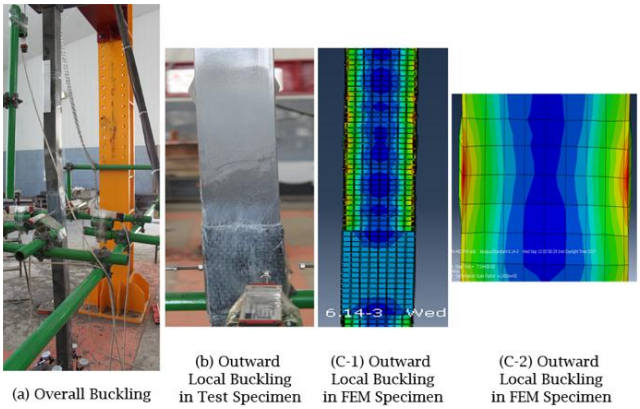

Fig. 18 Comparison the outward local buckling test and FEM in BOX80-DMG-MID-REC-CFRP

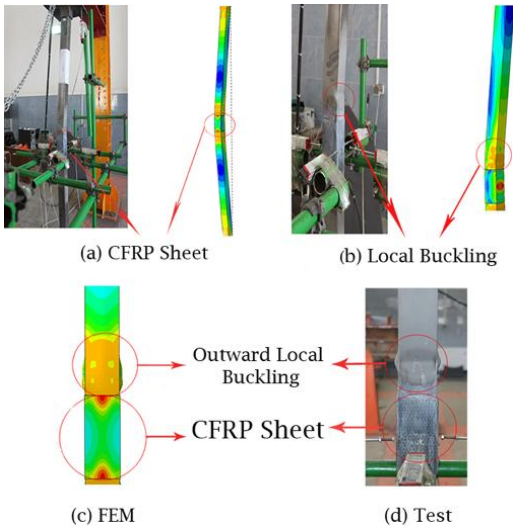

Fig. 19 Comparison of Overall-Local buckling test and FEM modeling in BOX80-DMG-MID-CIR-CFRP

sion until failure. Figs. 13 and 14 demonstrate the typical failure modes of BOX40 specimens. As for the non strengthening specimens, both inward and outward local buckling are observed in the deformed specimens while local buckling is prevented by the CFRP sheets regarding the retrofitting SHS with CFRP. Finally, Fig. 15 displays the CFRP layers which play an appropriate role in retarding or overcoming the local buckling in BOX40 columns. Based on the results in Figs. 17-19, BOX80 columns are inclined to greater local buckling prior to overall buckling due to the increase in (b/t). The results can provide the deformation obtained from the FEM analyses which is congruent with the experimental observations.

3.5 Influence of slenderness

Regarding the columns with smaller slenderness, the Cross Section of the columns is under compression. However, there is a region on the mid-height Cross-Section under tensile in the longitudinal direction for the columns with large slenderness. The load carrying capacity of specimens with deficient using CFRP in group #1 was smaller than that of the control sample. However, the load carrying capacity of specimens with deficient using CFRP in group #2 was almost the same as that of the control sample. The effect of increasing the slenderness ratio leads to a decrease in strengthening the effect of strength and ductility.

4. Conclusions

In the present study, 10 specimens of SHS steel columns including two types of damage were strengthened by CFRP sheets. Then, the effect of different parameters on the response of the Repaired columns such as the effect of the Cross-Section of deficient in column length, maximum load, stiffness values, and strengthening the effect of CFRP sheets were studied. In addition, Abaqus ver 6.14.1 as the finite element modeling program was used for the purpose of the study. The research findings lead to the following conclusions: (1) The finite element simulation results of the deformed mode of the steel columns agree well with the experimental results. The stress distributions of different specimens and failure modes have been analyzed, and the computed results show good agreement with the experimental results. (2) This study confirms that retrofitting methods are effective in expanding the local and overall buckling, decreasing stress around the damage location, and increasing the ductility. One unanticipated finding is that the BOX80 columns are inclined to greater local buckling prior to overall buckling due to the increase in $\left(\frac{b}{t}\right)$. (3) In BOX80 the applied CFRP layers were able to regain the strength to that of the undamaged strength of the section. (4) The stiffness caused by the maximum load-carrying capacity and maximum vertical were also investigated. The mean and standard deviation were calculated for both the lab and numerical modes. The results showed that the stiffness declined as a result of creating a deficient region. (5) The current study found that the CFRP strengthening is useful for overcoming the weakness and improving the performance of deficient intermediate steel SHS columns.

Acknowledgments

This study was financially supported by the Islamic Azad University, Zahedan branch, Iran and Construction Engineering Organization, Sistan and Baluchestan Province, Zahedan, Iran. The authors would like to appreciate everyone involved for their support.

References

Bambach, M. and Elchalakani, M. (2007), "Plastic mechanism analysis of steel SHS strengthened with CFRP under large axial deformation", *Thin-wall. Struct.*, **45**(2), 159-170.

Bambach, M., Jama, H. and Elchalakani, M. (2009), "Axial capacity and design of thin-walled steel SHS strengthened with CFRP", *Thin-Wall. Struct.*, **47**(10), 1112-1121.

Den, J., Jia, Y. and Zheng, H. (2016), "Theoretical and experimental study on notched steel beams strengthened with CFRP plate", *Compos. Struct.*, **136**, 450-459.

Devi, U. and Amanat, K. (2015), "Non-linear finite element investigation on the behavior of CFRP strengthened steel square HSS columns under compression", *Int. J. Steel Struct.*, **15**(3), 671-680.

Dieng, L., Amine, D., Falaise, Y. and Chataigner, S. (2017), "Parametric study of the finite element modeling of shot peening on welded joints", *J. Constr. Steel Res.*, **130**, 234-247.

Ghaemdoust, M., Narmashiri, K. and Yousefi, O. (2016), "Structural behaviors of deficient steel SHS short columns strengthened using CFRP", *Constr. Build. Mater.*, **126**, 1002-1011.

Karimian, M., Narmashiri, K., Shahraki, M. and Yousefi, O. (2017), "Structural behaviors of deficient steel CHS short columns strengthened using CFRP", *J. Constr. Steel Res.*, **138**, 555-564.

Kusnick, J., Benson, M. and Lyons, S. (2013), "Finite element analysis of weld residual stresses in austenitic stainless steel dry cask storage system canisters", Technical Letter Report; ML13330A512.

Narmashiri, K. and Jumaat, M. (2011), "Reinforced steel I-beams: A comparison between 2d and 3d simulation", *Simul. Model. Practice Theory*, **19**(1), 564-585.

Narmashiri, K., Jumaat, M.Z. and Sulong, N.R. (2010), "Shear strengthening of steel I-beams by using CFRP strips", *Sci. Res. Essays*, **5**(16), 2155-22168.

Park, J.W. and Yoo, J.H. (2013), "Axial loading tests and load capacity prediction of slender SHS stub columns strengthened with carbon fiber reinforced polymers", *Steel Compos. Struct., Int. J.*, **15**(2), 131-150.

Park, J.W. and Yoo, J.H. (2015), "Flexural and compression behavior for steel structures strengthened with Carbon Fiber Reinforced Polymers (CFRPs) sheet", *Steel Compos. Struct., Int. J.*, **19**(2), 441-465.

Park, J.W., Yeom, H.J. and Yoo, J.H. (2013), "Axial Loading Test and FEM Analysis of slender square Hollow Section (SHS) Stub Columns Strengthened with Carbon Fiber Reinforced Polymers", *Int. J. Steel Struct.*, **13**(4), 731-743.

Shahraki, M., Sohrabi, M.R., Azizyan, G.R. and Narmashiri, K. (2018), "Experimental and numerical investigation of strengthened deficient steel SHS columns under axial compressive loads", *Struct. Eng. Mech., Int. J.*, **67**(2), 207-217.

Sikadur-330 (2012), Product Data Sheet. Edition 21/02/2012, West Mead, South Africa.

Sikawrap-230C (2006), Product Data Sheet. Edition 13/06/2006, Adliya, Kingdom of Bahrain.

Teng, J.G., Yu, T. and Fernando, D. (2012), "Strengthening of steel structures with fiber-reinforced polymer composites", *J. Constr. Steel Res.*, **78**, 131-143.

Yang, Y., Chen, Z., Zhao, Z. and Liu, X. (2017), "Axial compression performance of steel box columns with different strengthening schemes", *Int. J. Steel Struct.*, **17**(2), 367-378.

Yousefi, O., Narmashiri, K. and Ghaemdoust, M.R. (2017), "Structural behaviors of notched steel beams strengthened using CFRP strips", *Steel Compos. Struct., Int. J.*, **25**(1), 35-43.

Zhou, X.H., Li, B.Y., Gan, D., Liu, J.P. and Chen, F. (2017), "Connections between RC beam and square tubed-RC column under axial compression: Experiments", *Steel Compos. Struct., Int. J.*, **23**(4), 453-446.

CC